P1.12

NUMERICAL SIMULATIONS OF THE EVOLUTION OF TROPICAL CYCLONE ELECTRIFICATION, LIGHTNING, MICROPHYSICS, AND DYNAMICS AT LANDFALL: PRELIMINARY RESULTS.

Alexandre O. Fierro*[1], Lance M. Leslie*[1], Edward R. Mansell*[2,3], Greg. J. Holland*[4], Jerry M. Straka*[1]
[1]School of Meteorology, Univ. of Oklahoma, Norman, OK
[2]Cooperative Institute for Mesoscale Meteorological Studies, Univ. of Oklahoma, Norman, OK
[3]NOAA/ NSSL, Norman, OK
[4]NCAR, Boulder, CO

1. INTRODUCTION

A Sophisticated cloud model featuring a 10-ICE microphysics scheme (Straka and Mansell, 2005) and a 3D branched lightning module (Mansell et al., 2002) explores the utility of a systematic monitoring of lightning activity such as flash rate, cloud to ground (CG) polarity and stroke multiplicity within tropical cyclones (TC), as they strengthen or weaken over the ocean and especially when they make landfall.

Many observational studies (e.g., Lyons et al. 1989; Molinari et al. 1994) have already stressed the importance of a more systematic monitoring of any change in TC lightning flash activity, as such activity is recognized as a very useful indicator of the distribution of convective precipitation within the TC. These findings suggest that knowledge of the evolution of the lightning flash activity (particularly within the TC eyewall) is extremely important at landfall, as it can be used to provide advance warnings for both potential flooding and other forms of severe weather.

2. EXPERIMENTAL DESIGN

The numerical simulations shown hereunder were performed up to 30 hours ahead on a 200x200x46 domain on an Arakawa C-grid having horizontal grid spacing $\Delta x=\Delta y=3$ km. The vertical grid stretches from $\Delta z=200$ m near the surface to $\Delta z=600$ m at and above 7 km AGL. The lightning grid spacing was set to 1.5 km. The model time step was 10 s.

The vortex and initial wind profile were initialized with a modified Rankine vortex having a radius of 280 km with maximum relative vertical vorticity of 1310^{-4} s^{-1}. With these parameters, the initial maximum horizontal winds were approximately 43 m s^{-1}. If the initial winds were weaker, a significant delay (in turn increasing computational cost) in the development of the convection (by frictional convergence) would occur and in some cases, the hurricane would fail to form. On the other hand (for the same initial vortex radius), initial winds greater than about 55 m s^{-1} would cause rapid development of scattered convection the domain, which ultimately dominate that of the eyewall, resulting in an early decline of the storm.

The following simulation was carried out on an f-plane with Coriolis parameter set to $3x10^{-5}$ s^{-1}. Lower values of f (e.g., < $2x10^{-5}$ s^{-1}) proved to show little difference with runs carried out with f set to zero. Early test runs revealed that not including f resulted in rapid development of unusually strong convection around the eyewall, leading to a rapid demise of the TC. The larger the value of f, the weaker the convection in and around the eyewall. Moreover, as f increases the diameter of the eyewall increases as additional supply of planetary vorticity is constantly ingested into the storm, acting has an additional source of angular momentum.

The surface pressure at sea level is set to 1011 mb everywhere across the domain and the sea surface temperature is set to 28°C.

For the electrification, a simple non-inductive (NI) graupel-ice scheme was selected where the magnitude of collision was multiplied by $9x10^{-4}$ in order to significantly reduce the computational cost associated with an overall large intra-cloud (IC) lightning flash activity (> 300 flashes per minute). For these reasons, very few IC flashes are observed above 9 km in the simulation. On the other hand, inductive graupel-droplet charging, which may be involved in generating lower-altitude charge regions (Mansell et al. 2005), was set to weak to moderate values.

In order to assess the impact of the land mass on the storm's microphysics and lightning evolution, two simulations were carried out for this analysis: one without land (e.g., ocean run) and one with an idealized landmass. The land or coast is represented by a meridionally (i.e. North-South) oriented slab moving towards the east at a constant translation speed set to 8 m s^{-1} "towards" the center of the domain where the center of circulation of the TC is located. In order to keep the TC from moving away from the center of the domain the translation speed of the domain was set to constant values of u = - 2.5 m s^{-1} and v = 1.5 m s^{-1}. The land mass "starts" to enter the western portion of the domain at t ≈ 10h 30 min. In this model, momentum flux is enhanced over land, while the sensible heat and moisture flux are suppressed.

Initial Conditions

The initial environmental conditions were represented by a composite sounding of the 00 UTC Owen Roberts Airport, Grand Cayman sounding below z = 15 km and the 00 UTC Kingston, Jamaica sounding of August 13th 2004 above that level (Fig 1). This procedure was carried out because the environments from both soundings showed great similarities above 15 km. At that time, Hurricane Charley passed over or near the islands (less than 100 miles) and was rated as a Category 3 on the Saffir-Simpson scale.

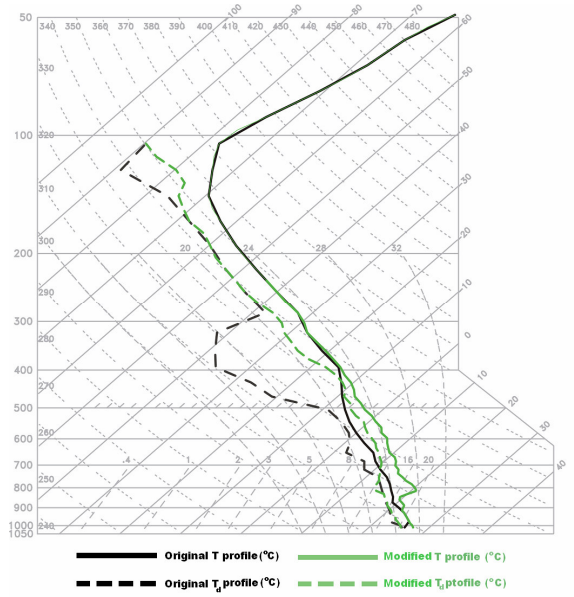

Figure. 1. Original (black) and modified (green) composite Skew-T log-p diagrams of the 13th August 2004, 00UTC Owen Roberts airport, Grand Cayman and 00 UTC Kingston, Jamaica.

As shown in Fig.1, the original composite sounding was modified in order to optimize the chances for a well-defined hurricane to form. The dry layer between 300 and 500 mb was removed so has to reduce evaporative cooling and hence downdraft strength at these levels. Also, between 700 and 850 mb, a capping inversion layer was added in order to prevent convection within the bands from developing too rapidly. The cold air intrusion from the convective cell's strong downdrafts has been shown to cause the convection within the eyewall to weaken and ultimately to dissipate. Elsewhere, the relative humidity was preserved to a lesser extent so as to prevent further downdraft enhancement. After these modifications, the CAPE and CIN values of the model sounding (i.e., when interpolated to the grid) were of about 1473.6 and 99.2 J kg^{-1}, respectively (compared to 1560 and 22.1 J kg^{-1} in the original composite sounding).

3 RESULTS AND DISCUSSION

1. Kinematic and microphysics evolution.

During the simulation, the vortex goes through several phases, the first being a rapid development of convection in concentric rings around the center at about 2.5-3 h (mainly caused by using a homogeneous environment as initial condition). As time progresses, the individual convective elements organize around the center to form a broad ill-defined eye around 9 h. Later on, the eyewall continues to shrink and is coincident with a progressive deepening of the central pressure at z = 1 km AGL (Fig. 2).

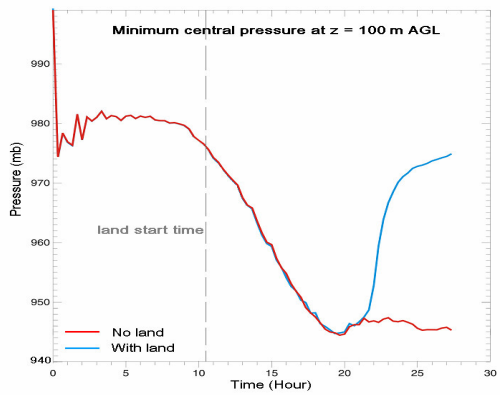

Figure. 2. Time-height plot of pressure at z = 100 m AGL for the first 27.5 hours of simulation. Blue (red) line shown for the land (no-land) case.

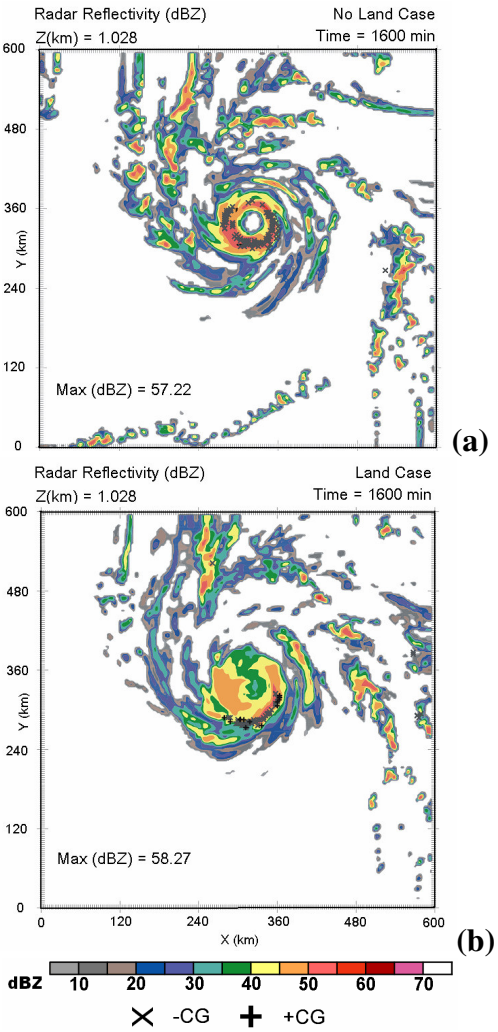

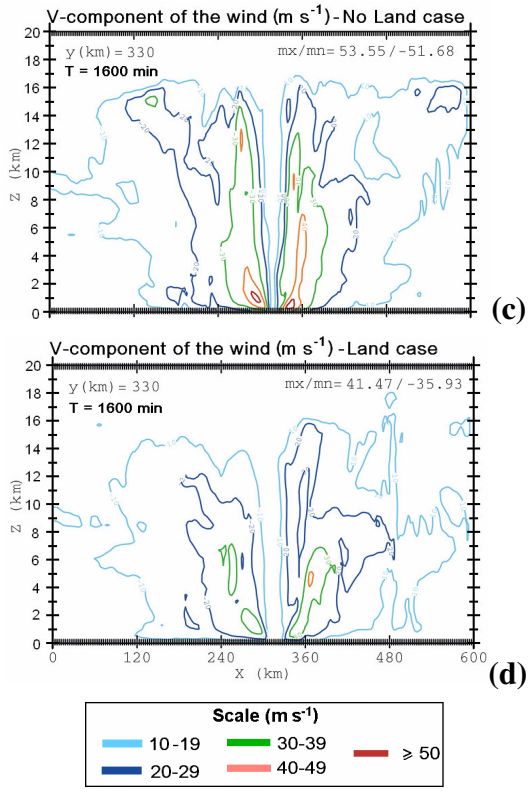

Figure. 3. (a) and (b) Horizontal cross section of radar reflectivity (dBZ) shown by 5 dBZ contour increments from 5 dBZ to 75 dBZ at t = 1600 min for (a) the ocean and (b) the land case, at z = 1,017 km. Locations of CG lightning strikes are also shown by a cross for –CG flashes and by a + symbol for +CG flashes. The flash locations were plotted for 6000 s time interval from the cross section time. Panels (c) and (d) show vertical cross section in the X-Z direction of the V (or Y) component of the wind field at y = 330 km, with corresponding scale shown below.

After 8 hours, the central pressure at 100 m drops progressively to reach a minimum of ~945 mb at about 19.5 h (Fig. 2), corresponding to the typical pressure observed in a Category 3 storm. The sudden pressure drop from 999 mb to about 975 mb at the start of the simulation (Fig. 2) is likely caused by a rapid hydrostatic (geostrophic) adjustment response of the model to the Rankine vortex imposed as initial wind field.

As expected, the TC significantly weakens once the eyewall is completely over land at about 21.5 h. The minimum central pressure at z = 100 m AGL experiences a sharp and relatively fast increase of ~30 mb in less than 5 h (Fig. 2).

At 26 h 40 min (1600 min) of simulation time, the vortex shows a distinct eyewall with several connecting rainbands (Fig. 3a).

At that time, tangential winds exceed 50 m s^{-1}, with the highest gusts just within the boundary layer above ground (Figs. 3c), corresponding to a low-end Category 3 storm.

Consistent with many *in situ* observations the TC eyewall exhibits an outward tilt in reflectivity (at lower levels, Fig. 4) and tangential wind profile (Fig 3c).

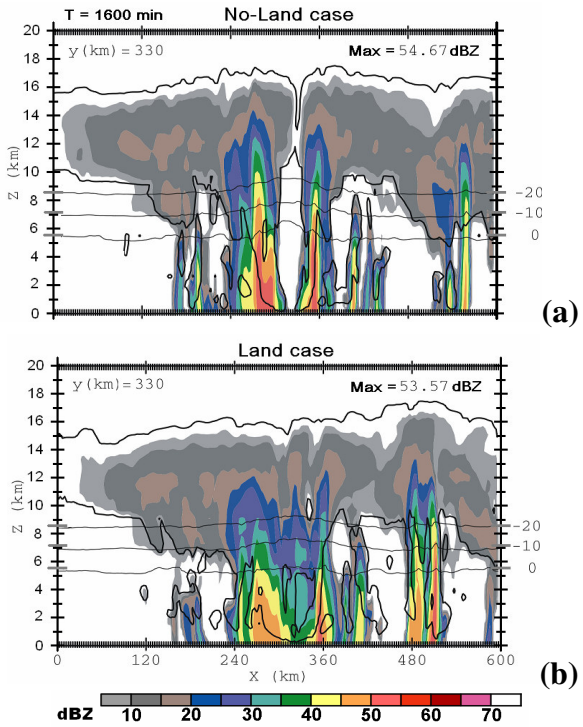

Figure. 4. Vertical cross sections of radar reflectivity (dBZ) at 5 dBZ contour intervals from 5 dBZ to 75 dBZ at t = 1600 min (taken at y = 330 km) for (a) the ocean and (b) the land case. The thick black lines show values of cloud mixing ratio of 0.1 g kg^{-1}, which depicts the cloud boundary.

Maximum meridional (tangential) wind component are exceeding 50 m s^{-1} over ocean, while remaining below 40 m s^{-1} once over land at the same time (compare Figs. 3c and 3d). The horizontal and vertical reflectivity profile of the TC over land show many features consistent with *in situ* observations, namely, overall weaker reflectivity in and around the eyewall and the absence of a closed circular eyewall and eye near and around the storm's center (Figs. 3b and 4b). This is a consequence of weaker updraft mass flux in the eyewall and hence weaker divergence aloft, in turn reducing the subsidence and the subsequent warming responsible for the formation of the eye. On the other hand, when the storm evolves over open waters, more continuous convection in the eyewall and a well-defined closed circular eye are noticeable near the storm's center, (Figs. 3a and 4a). Between these two convective regions, a stratiform region with weak reflectivity values at lower levels is also observed (e.g., see Fig. 4a at x = 390 km). Weak secondary bands underneath the outer core stratiform region of the storm's eyewall are also found on the storm's western and eastern flank (e.g., Figs. 4a at x = 200 km and x = 400 km.).

Moderate hail and graupel mixing ratios are primarily found within the eyewall and within the individual convective cells forming the outer rainbands (Fig. 5).

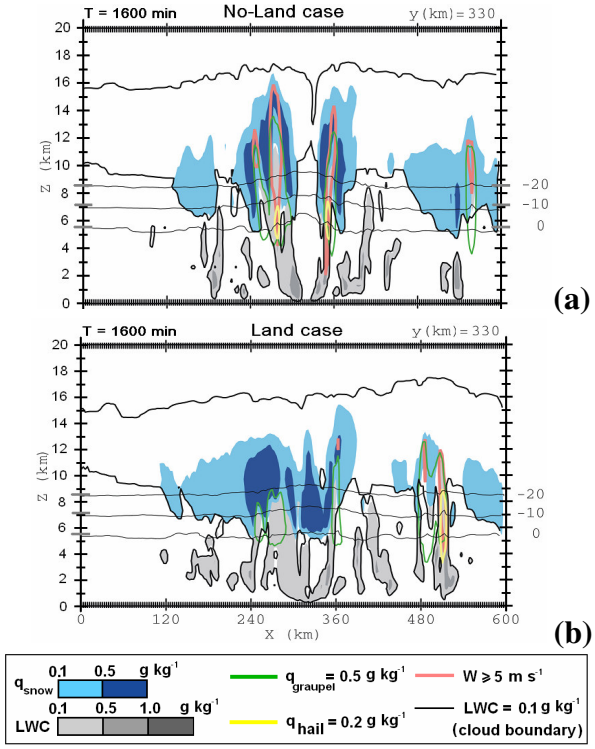

Figure. 5. As in Fig. 4 for LWC, snow mixing ratio, total hail mixing ratio and total graupel mixing ratio. The black thick line depicts the cloud boundary (0.1 g kg^{-1} cloud mixing ratio). LWC is shown in shaded with scale shown by the legend below the panel. Green (yellow) contours depict regions of the storm where the total graupel (hail) mixing ratio exceeds 0.5 g kg^{-1} (0.2 g kg^{-1}). Light (dark) blue-filled area shows snow mixing ratios greater than 0.1 g kg^{-1} (0.5 g kg^{-1}).

The lighter ice crystals and snow particles nucleating inside the eyewall are advected radially outward to form a weak-echo stratiform region, commonly referred as the outer eyewall (e.g., Fig. 4a at x = 390 km).

Meanwhile, it is also interesting to note that the 0°C and –20°C isotherms are found at higher altitude inside the eye (e.g., Fig. 5), which is consistent with hurricane being warm core lows. In the land case simulation, these isotherms show a much less pronounced sloping, which is consistent with less subsidence in a much a weaker storm.

It is well established that in oceanic convection, the strong updrafts able to produce graupel/hail particles are usually found above the mixed phase region (defined as the layer between the 0°C and –20°C isotherm) due to less unstable environments and weaker surface forcings. In the simulations, the great majority of updrafts exceeding 5 m s^{-1} are also found above that level (Fig. 5a). Moreover, the smaller concentration of cloud condensation nuclei (CCN) over oceans causes the droplet spectrum in maritime clouds to have fewer small droplets (of radius < 10 μm) and more large droplets (of radius > 20 μm). Hence fewer smaller and lighter droplets will be available in maritime clouds for the formation of graupel pellets within the mixed-phase region, which are necessary for sufficient charging to occur. In other words, observational evidence supports the hypothesis that oceanic convective systems are overall weakly electrified.

The presence of hail is collocated with moderate cloud mixing ratios ranging between 0.1 and 0.5 g kg^{-1} (Figs. 5), which as expected, are found nearby relatively moderate to strong updrafts (see pink contours in Figs. 5) in the mixed phase region. Furthermore, the regions of the TC having stronger updrafts are also associated with larger LWC due to enhanced condensational heating. Hence, these confined regions within the storm are more conducive for collisional non-inductive (NI) charging processes between graupel/hail and lighter ice crystals.

Indeed, charging able to produce lightning occurs within the strongest cells forming the TC outer rainbands and the storm's eyewall (Fig. 6).

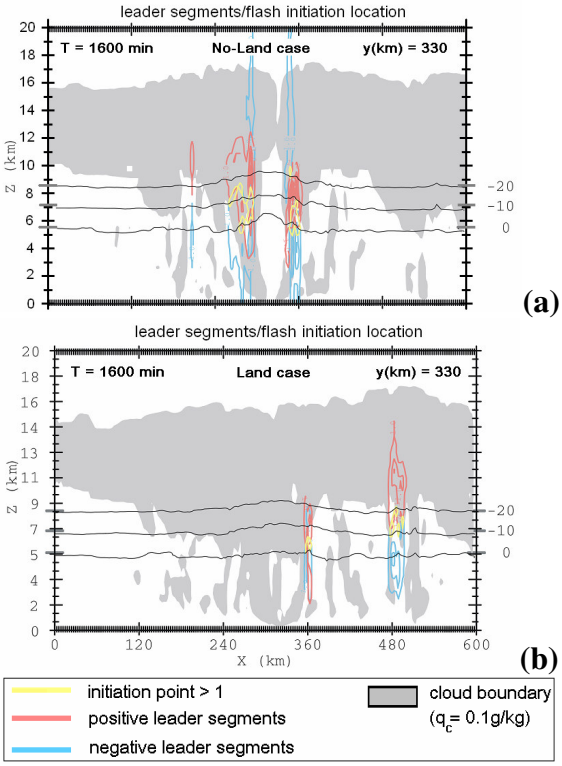

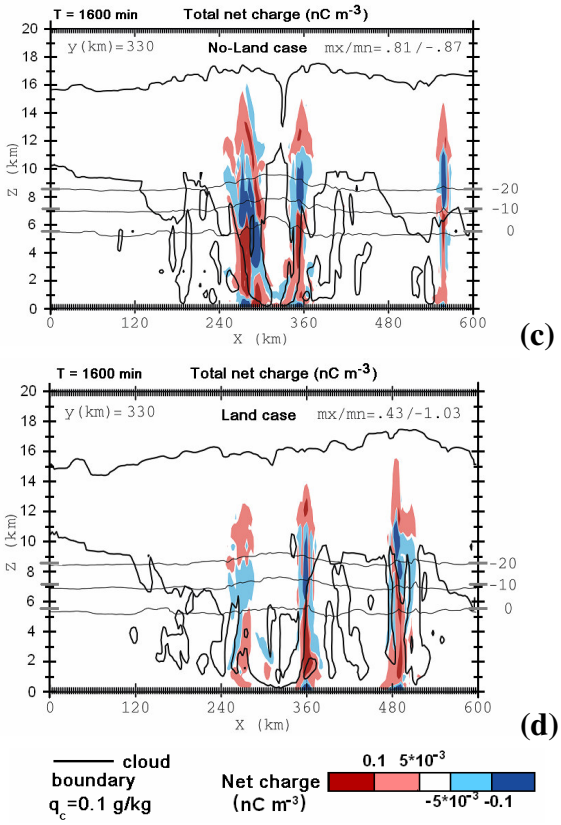

Figure. 6. Vertical cross section (as in Fig. 4) of cloud mixing ratio (grey shaded area), positive (negative) leader segments in red (blue) contours for (a) the ocean and (b) the land case. The leader contours starts at 1 by increments of 10. Yellow contours show flash initiation locations greater than 1. Also shown are the net charge density in nC m^{-3} for (c) the ocean and (d) the land case. Light (dark) red filled contours show region where charge exceeds 5X10^{-3} (nC m^{-3}). Likewise light (dark) blue filled contours shows where negative values exceed magnitudes of 5X10^{-3} (nC m^{-3}), respectively.

Before carrying out the analysis of the electrification, it is noteworthy to mention, however, that the NI and inductive charging vertical profiles (not shown here) and the vertical net charge structure plots shown in Figs. 6c and 6d are only snapshots at a specific location of the storm and consequently do not provide an exhaustive representation of the charging and net charge profile within the storm at all times and locations.

Relatively strong positive inductive charging occurs at midlevels in the mixed phase region of the eyewall (not shown). This is the most likely primary cause of the formation of the lowest positive charge layers below 5 km (Figs. 6c and d) as some of these positively charged graupel in the mixed phase region will ultimately fall below the melting level ($z \approx 5$ km), while keeping most of their charges gained aloft. The magnitude of the positive NI charging on graupel in the mixed phase region is however relatively small compared to that of negative NI charging that is observed above this region and compared to that of inductive charging at the same level (not shown).

If the NI multiplier was set to a much higher value (e.g., 0.1), much larger amount of charge would overall be attributed to NI charging rather than inductive charging (even for moderate values of inductive charging), in turn resulting in a much stronger mid-level (and upper level) negative (positive) charge region. The heavier graupel particles in the mixed phase region will be left with a net negative charge, while the lighter ice crystals colliding with it will carry larger amount of net amount of positive charges in the upper level cirrus forming the TC stratiform region. This in turn would cause much larger electric fields at mid-to-upper levels of the storm in turn resulting in much higher IC flash rates at these levels (> 300 flashes per min).

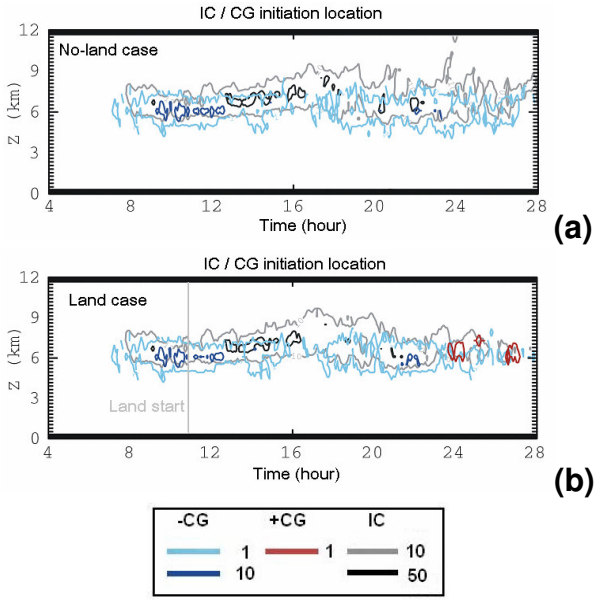

Figure. 7. Time-height plot (i.e., horizontally integrated through the entire domain) of the IC and +/- CG initiation location for the first 28 hours of simulation for (a) the no-land case and (b) the land case. The land start time is indicated by a light grey line in panel (b).

It is interesting to notice that once the storm has significantly weakened over land after 24 h, a few +CGs are observed in the southern portion of the eyewall, whereas no +CGs are produced in the ocean case. A closer analysis (from additional cross sections not shown here) reveals that these +CGs are generated within a few storm cells embedded the southern eyewall that exhibit an inverted triple charge structure (a main positive charge region amidst two negative ones). Since in these simulations NI charging is set to very weak values compared to that of inductive charging, this inverted tripole is mainly due to induction (not shown). In these cells, relatively strong negative charge (i.e. > 10^{-1} nC m^{-3}) extends all the way to the ground (after sedimentation from the upper mixed-phase region) and is collocated with positive leaders propagating all the way to the ground (not shown).

The differences between the simulations over ocean than the one with land becomes more evident after 22 h (e.g., see Fig. 2). The land case shows overall much weaker total updraft mass flux extending over a weaker depth than the ocean case (not shown). This weaker total updraft mass flux is correlated in time with smaller total graupel volume (not shown) due to less lofting and lower LWC in overall weaker, shallower updrafts in the eyewall (e.g., Fig. 5 for a snapshot). As a result, less total charge will be separated in the eyewall, leading in a progressive decrease in the total lightning activity within the storm (compare Fig. 7a and b).

3. CURRENT ISSUES AND FUTURE WORK

Currently, two major issues remain for the completion of a "successful" simulation.

The first problem is related to the storm internal dynamics and kinematics: Once a well-defined eyewall and spiral rainbands start to appear after the initial convective burst near and around the Rankine vortex center, the TC start to weaken near after 30 h of simulation (using identical electrical, microphysical and kinematical parameters). After 30 h, the outer rainbands start to dominate the convection near the center and start to expand in area to form local small storm clusters. Ultimately, these clusters generate strong cold pools, along which they will tend to propagate. After 3 hours, the bands and cluster of storms once forming the rainbands have completely propagated away from the eyewall. However, the detrimental effect of the low θ_e air from these cold pools does not seem to be the primary cause for the weakening of the eyewall convection. Rather, further analysis showed that the regions around the eyewall void of convective activity at LCL level (between 1 and 1.7 km) are characterized by warm temperature anomalies exceeding 2-3 K which are not present at earlier times (5 hours earlier, not shown). This generalized stabilization of the atmosphere at these levels is apparently not caused by large scale subsidence across the domain. It is possible that the inclusion of radiative cooling via a radiative model could help in minimizing this generalized warming of the atmosphere as the latter acts to cool down the atmosphere at the same time scale.

The second major problem is related to the storm microphysics and electrification parameterizations. One of the major caveat of the microphysics used in this simulation is the lack of ability to predict explicitly ice particle concentration in turn causing an overestimation of the latter (due partly to enhanced contact freezing) and a resulting high total (horizontally integrated) IC flash rate (> 300 per minute) at upper levels (i.e. above 9 km). That is why, in the future, an improved version of the code featuring explicit prediction of ice particle concentration rather than an *ad hoc* diagnosis would improve in reproducing lower and more realistic ice particles profiles in the storm. This in turn, would allow the use of a higher and more realistic NI multiplier. With these parameters, the evolution of the total IC flash rate (particularly in the eyewall) could be diagnosed as the latter was shown to be as a good indicator of convective strength (e.g., MacGorman et al. 1989 for the Great Plains supercells) and hence for convective burst events associated with potential imminent strengthening of the TC. An important limiting factor of these simulations is also the rather high computational cost of the calculation of the lightning flash channel propagation at each time step, which stresses the importance and attractiveness of reproducing lower (and also more realistic) IC flash rates.

Higher resolution simulations are currently on their way on the new Itanium® high-performance supercomputer at the Oklahoma Supercomputing for Education and Research (OSCER) center in Norman. Furthermore, a Message Passing Interface (MPI) version of the model code is scheduled for the future for simulation at higher resolution.

Future work will include the following:

- A land mass with limited width in order to analyze the influence of the land width in proportion to the storm weakening.
- A constant basic current (or even current with directional/speed shear).
- The beta effect for a more realistic background flow.

Acknowledgements: We thank the Organization of Naval Research (*ONR)* for generously sponsoring Alexandre Fierro (Grant N00014-02-1-0181); and The Oklahoma Supercomputing Center for Education and Research (*OSCER)* for providing the computing resources. Partial support for this research was also provided by the National Science foundation *(NSF)* under grants ATM-0119398 and ATM- 0340693

REFERENCES

Black, R. A. and J. Hallett, 1999: Electrification of the hurricane, *J.Atmos Sci*, **56**, 2004-2028.

Lyons, W.A., M.G. Venne, P.G. Black and R.C. Gentry, 1989: Hurricane lightning: A new diagnostic tool for tropical storm forecasting? Preprints, 18th Conf. on Hurricanes and Tropical Meteorology, San Diego, American Meteorological Society, 2 pp.

MacGorman, D. R, D. W. Burgess, V. Mazur, W. D. Rust, W. L. Taylor and B. C. Johnson, 1989: Lightning rates relative to tornadic storm evolution on 22 may 1981. J. Atmos. Sci., 46, 221-250.

Mansell, E. R., D. R. MacGorman, C. L. Ziegler, J. M. Straka, 2002: Simulated three-dimensional branched lightning in a numerical thunderstorm model, *J. Geophys. Res*., 107 (9), 4075, doi:10.1029/2000JD000244.

Mansell, E. R., D. R. MacGorman, C. L. Ziegler, and J. M. Straka (2005), Charge structure and lightning

sensitivity in a simulated multicell thunderstorm, *J. Geophys. Res.*, **110**, D12101

Molinari, J., P.K. Moore, V.P. Idone, R.W. Henderson, and A.B. Saljoughy, 1994: Cloud-to-ground lightning in Hurricane Andrew. *J. Geophys. Res.*, **99**, 16665-16676.

Molinari, J., P. Moore, V. Idone, April 1999: Convective structure of hurricanes as revealed by lightning locations, *Mon. Wea. Rev.*, **127**, 520 - 534.

Straka, J. M. and E. R. Mansell, 2005: A bulk microphysics parameterization with multiple ice precipitation categories. Accepted in *J. Appl. Meteor.*